Signal diversity for the reduction of signal dropouts and speckle noise in a laser-Doppler extensometer

Fangjian Wang[a,*], Steffen Krause[b], Christian Rembe[a]

[a]*Institute for Electrical Information Technology, TU Clausthal, Leibnizstraße 28, Clausthal-Zellerfeld, 38678, Germany*

[b]*SincoTec Test & Engineering GmbH, Freiberger Straße 13, Clausthal-Zellerfeld, 38678, Germany*

Abstract

A recently demonstrated laser-Doppler extensometer is affected by signal dropouts caused by speckle noise, whereby the carrier-to-noise ratio (*C/N*) falls below the so-called frequency-modulation threshold. In this article, we present a new optical setup with polarization signal diversity for reducing speckle-induced dropouts dramatically. The probability of a signal dropout can be substantially reduced using weighted combination signals from different photodetectors collecting the scattered light at two orthogonal polarizations. Therefore, we prove in this paper that signal diversity enables a laser-Doppler extensometer for industrial applications. Furthermore, a theoretical model based on the speckle statistics for estimating the probability of signal dropout is introduced. The relationship between the occurrence of signal dropouts and the demodulation bandwidth is studied. The experimental results of the occurrence of dropouts highly match the theoretical estimated probability distribution. Finally, strain measurement demonstrates a significant reduction of speckle noise with the implemented technique.

Keyword: laser-Doppler extensometer; in-plane laser-Doppler vibrometry; laser speckle; signal diversity; polarization diversity; speckle-insensitive laser vibrometry

1. Introduction

In-plane laser-Doppler vibrometers (LDV) [1,2] are widely used to measure the instantaneous velocity of a solid surface [3] and to analyze vibrations [4]. Due to the contactless measuring principle and the real-time capability with a high bandwidth of the vibrometer, the laser-Doppler technique can measure vibrations in a wide frequency range from a few mHz [5] to GHz [6]. Recently, we presented a new type of laser-Doppler strain sensor, a so-called laser-Doppler extensometer [7]. This sensor measures the displacements of two adjacent measuring points simultaneously, subtracts the displacement signals in the digital domain, and divides the differential displacement by the distance of two measurement points. For each measuring point, the displacement is measured according to the principle of heterodyne in-plane laser-Doppler vibrometry. The measured in-plane velocity is proportional to the Doppler frequency shift (the difference between the frequencies of the Doppler signal and the carrier). The measured displacement is proportional to the phase of intensity modulation (corresponding to the integration of Doppler frequency shift). Our sensor can be used in all strain-measurement applications where strain gauges are employed if the surface scatters light and is optically accessible. Strain measurements in machines or on constructions outside are such examples. Even though our sensor was integrated into a resonance-testing machine and

provided comparable measurement results as a common strain gauge, it is affected by signal dropouts due to speckle noise [7]. Signal power is reduced if less light power scatters into the detection aperture as a result of a dark laser speckle [8]. A signal dropout occurs if the carrier-to-noise ratio (*C/N*) of the photodetector signal falls below the frequency-modulation (fm) threshold. Thus, a drop below the fm threshold defines a dark speckle. The *C/N* is the carrier power in relation to the total noise power within the demodulation bandwidth. The demodulation bandwidth in respect to the Carson rule [9] is determined by the sensor-signal bandwidth and the maximum Doppler frequency shift, which is proportional to the maximum in-plane velocity to be measured. Only the noise in the demodulation bandwidth is relevant for the demodulated signal. The noise outside this bandwidth can be filtered by an analog or a digital filter before demodulation. In practice, the concrete fm threshold depends on several factors, such as demodulation algorithms or modulation index. The threshold at a value for the *C/N* of *C/N*=1 is achievable for an ideal demodulator and a modulation index close to zero [10]. The threshold is usually at higher values of the *C/N* when these conditions are not met. However, the modulated signal can be obtained correctly if the condition *C/N* is higher than the fm threshold. At a *C/N* below the fm threshold (in case of a signal dropout), the demodulated signal contains only noise, since the increase of noise in the photodetector signal shows a disproportionate increase of the noise in the demodulated signal [11].

By measuring small strain in a resonance test machine (as in our previous article [7]) the laser speckle remains nearly constant during the strain measurement and, therefore, also the *C/N* of detector signals remains mostly at one level. Thus, in this case the speckle noise mainly affects the setup effort before starting the measurement. The sensor must be adjusted until the *C/N* at either measuring point is above 1. Non-contact measurement methods should allow a quick setup compared to tactile sensors but the requirement of searching for bright speckles reduces the advantage dramatically. This problem becomes more critical for measuring large strains, when the assumption of a constant *C/N* is no longer valid. In this case, speckles vary continuously und randomly during the measurement. Signal dropouts corresponding to noise bursts in the demodulated velocity signal and phase distortions in the demodulated displacement signal generate additional noise and, consequently, measurement errors.

This problem is known from in-plane LDV [12,13], but was mainly demonstrated for out-of-plane LDV [14] so far. However, the speckle noise in out-of-plane LDV, which appears when additional in-plane motion is present, were widely studied [15-17]. Most of these solutions can also be applied to in-plane LDV. The most efficient solution among them is signal diversity. The diversity technology was implemented first to improve signal quality in communication technology [18-20]. The signal is transmitted via several stochastically independent channels, whereby the simultaneous occurrence of errors in such channels is extremely improbable. This allows the signal to be received as error-free as possible. In common LDV, signal diversity was introduced to reduce signal dropouts and speckle noise [21-23]. Polarization, detection-angle (different apertures for the receiving channels) or wavelength diversity can produce statistically independent speckle patterns [8] and, thus, independent detector signals. The probability of signal dropouts occurring simultaneously by two independent signals is significantly reduced compared to a single channel. If we weight and combine statistically independent signals, most of the signal dropouts can be avoided and the speckle noise can be substantially reduced. Based on our previous sensor structure, it was much easier for us to implement polarization diversity, requiring only a few additional optics and preserving the main

optical setup. It provides the simplest optical setup for a compact extensometer design. Detection-angle diversity [24] would require additional receiving optics, and wavelength diversity would require a second laser source. Thus, we give the highest priority to the implementation of polarization diversity. When linearly polarized incident light is diffracted by a rough metallic surface, the speckle patterns observed at two orthogonal polarizations may be more correlated than in the case of a rough dielectric surface [8]. Metal surfaces appear often in strain measurements with resonance test machines. Therefore, we used an aluminum specimen with a rough surface and investigated whether independent speckle patterns were generated by light in different polarizations. Our first experimental result proves that polarization diversity produces stochastically independent speckle patterns on such surface. Furthermore, we construct a theoretical model based on the speckle statistics to estimate the probability of signal dropouts related to the demodulation bandwidth. The experimental results of the occurrence of signal dropouts are in good agreement with the estimated value and demonstrate that polarization diversity substantially reduces the probability of signal dropouts. As a result, the occurrence of signal dropouts can be reduced using signal diversity. Here we focus on the effect of the signal dropout. Because in this case the strain cannot be measured. All the cases with *C/N* above 1 are considered equally. Practically, the higher the *C/N* of the modulated signal, the higher the signal-to-noise radio (*S/N*) of demodulated signal. The *S/N* of the demodulated signal for the case without signal dropouts (*C/N* above the fm threshold) increases linearly with the *C/N* of the modulated photodetector signal [11]. Moreover, the reduction of signal dropouts and speckle noise is also shown in the time domain. Finally, the results of strain measurement demonstrate that signal diversity can significantly reduce the speckle noise in laser-Doppler extensometers.

In our previous publication [7], we proved that our extensometer without signal diversity measures strain in the resonance-testing machine correctly at bright speckles, but it was still affected by the problem of signal dropouts at dark speckles. This problem drastically restricts the advantage of a quick setup compared to tactile sensors and could cause huge measurement errors (especially measuring large strains). In this paper, we demonstrate that the effect of signal dropouts and speckle noise can be significantly reduced by using signal diversity. Therefore, we are confident that our laser-Doppler extensometer can be manufactured for industrial applications and replace traditional strain gauges on a large scale for measuring dynamic strain.

2. Methods

2.1 Limits of the prior laser-Doppler extensometer

Our prior laser extensometer [7] measures in-plane displacements of two adjacent points and the strain is computed from the relative displacement divided by the distance between these two points (named as measuring points in the following text). The basic measurement principle for each measuring point is a heterodyne in-plane laser-Doppler vibrometer (in figure 1).

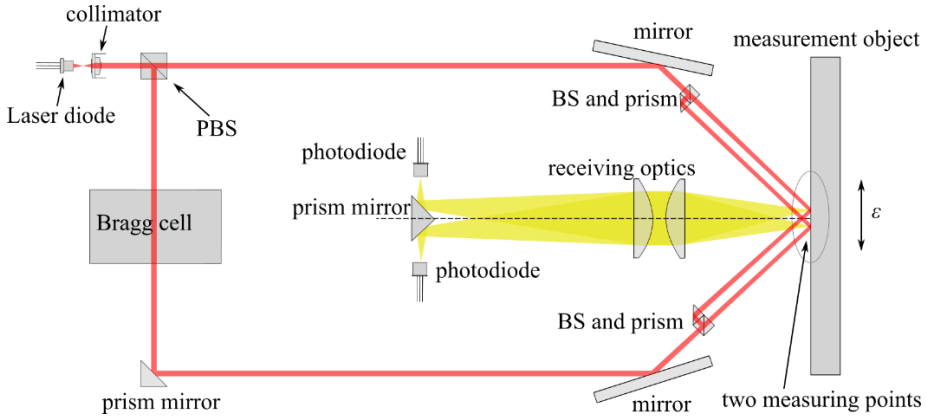

Figure 1: Schematic drawing of the previous optical setup without polarization diversity [7].

Two laser beams from a single laser diode superimpose on the surface of the specimen and create an interference fringe pattern. One beam is frequency shifted and a carrier signal is generated at a frequency of 40 MHz, allowing detection of the direction of in-plane motions. The scattering body of the rough surface moves through the fringe pattern and modulates the light power scattered in direction of the photodetector. Usually, several scattering bodies move through the fringe pattern and the interference of the scattered light fields creates a speckle-pattern. The scattered light is collected by a lens system and finally detected by photodiodes. Since the modulation frequency can also be derived by the interference of two Doppler-shifted beams, the high-pass filtered photodetector signal amplified by a transimpedance amplifier (TIA) is given without noise by

$$u_s(t) = \sqrt{2} K_{PD} P_0 R_g \gamma \sin\left(2\pi f_c t + \phi(t)\right). \tag{1}$$

Here, K_{PD} is the sensitivity of the photodiode, γ the interference efficiency ($\gamma = 1$ for perfectly matched wavefronts), P_0 is the effective power of the intensity modulation on the photodiode, R_g is the feedback resistance of the transimpedance amplifier, f_c is the carrier frequency and $\phi(t)$ is the phase of the interference signal, which corresponds to the integration of the Doppler-frequency-shift (the difference between the frequencies of the Doppler signal and the carrier). The in-plane displacement can be derived by analyzing the phase (here $\phi_1(t)$ for the first measuring point and $\phi_2(t)$ for the second). Finally, the strain $\varepsilon(t)$ measured by our extensometer is given by (see our previous publication [7])

$$\varepsilon(t) = \frac{d}{2\pi l}\left(\phi_1(t) - \phi_1(t_0) - \phi_2(t) + \phi_2(t_0)\right). \tag{2}$$

Here d is the distance between two nearby fringes, l is the distance between the center of two measuring points, and t_0 is the starting time.

However, the measurement results with our previous design were strongly affected by the speckle noise and the signal dropouts. Figure 2 shows the amplitude of the carrier signals and the noise floor at 3 random positions on the surface of the specimen using the prior sensor design [7]. The strength of carrier signal (peaks at 40 MHz in figure 2) varied with the measuring positions. Both carrier signals had sufficient strengths only at position 1, with the overall *C/N* exceeding 1 in the 1 MHz demodulation bandwidth.

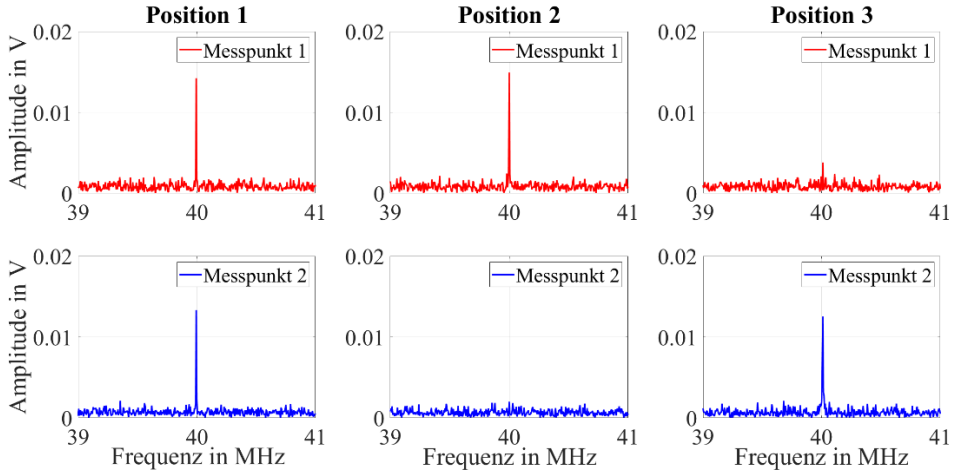

Figure 2: Spectrum of the carrier signals detected by the photodiodes for both measuring points (the 1st measuring point upper and the 2nd lower) at 3 random measuring positions (position 1, 2 and 3) on the surface of the specimen. Resolution bandwidth (RBW) = 5 kHz.

Here the *C/N* can be calculated with the signal power P_s according to equation 1 and with the noise power P_n by

$$\frac{C}{N} = \frac{P_s}{P_n} = \frac{u_s^2}{u_n^2} = \frac{K_{PD}^2 P_0^2 R_g^2}{u_n^2} \tag{3}$$

where u_n is the voltage noise in the demodulation bandwidth. At the position 2 and 3, the carrier amplitude of one Doppler signal was nearly equal to or below the noise floor. The strain is not measurable at these both positions. Therefore, a new speckle-insensitive optical design was required. In this paper, we present for the first time a design of a laser-Doppler extensometer with signal diversity. We explore the reduction of signal dropouts for our new solution and discuss the noise reduction through signal diversity in this paper.

2.2 Polarization diversity

In general, polarization, detection-angle or wavelength diversity can be implemented to solve the dropout problem mentioned above. Polarization diversity enables the most compact solution, requires only few additional optics, and preserves the main optical setup of our previous structure. Perpendicular scattering from a plane metal surface maintains the polarization direction. However, in the case of scattering with an angle, the polarizations have different scatter behavior. For a rough surface, independent speckle fields can be expected for two orthogonal polarization states as demonstrated below. Since interference can only occur at the polarization of the reference beam, the orthogonal polarization state in respect to the polarization of the first reference beam can be used for another diversity channel. Angular diversity limits the numerical aperture (NA) of each receiving channel because the aperture needs to be shared. For wavelength diversity, the laser power of each wavelength should be halved considering the laser safety class. Therefore, the optical structure can only be implemented with polarization diversity without significant *C/N* loss of the individual photodetector signal. Polarization diversity requires two uncorrelated speckle fields represented by the two orthogonal polarization states. To prove the correlation behavior, the *C/N* of both diversity channels at *N* different positions on the metal surface of the specimen was measured. Then, two vectors $\underline{C/N}_1$ and $\underline{C/N}_2$ were obtained, where $\underline{C/N}_1[n]$ is the *C/N* of the first diversity

channel at position n in a resolution bandwidth of 1 Hz and $\underline{C/N}_2[n]$ is the *C/N* of the second channel at the same position but with orthogonal polarization. The cross correlation of these two vectors was calculated using the formula

$$\underline{R}_{\underline{C/N}_1,\underline{C/N}_2}[m] = \begin{cases} \dfrac{\sum_{n=1}^{N-m}\left(\underline{C/N}_1[n+m]-\overline{\underline{C/N}_1}\right)\left(\underline{C/N}_2[n]-\overline{\underline{C/N}_2}\right)}{\sqrt{\sum_{n=1}^{N}\left(\underline{C/N}_1[n]-\overline{\underline{C/N}_1}\right)^2\sum_{n=1}^{N}\left(\underline{C/N}_2[n]-\overline{\underline{C/N}_2}\right)^2}}, 0 \le m < N \\ \dfrac{\sum_{n=1}^{N+m}\left(\underline{C/N}_1[n]-\overline{\underline{C/N}_1}\right)\left(\underline{C/N}_2[n-m]-\overline{\underline{C/N}_2}\right)}{\sqrt{\sum_{n=1}^{N}\left(\underline{C/N}_1[n]-\overline{\underline{C/N}_1}\right)^2\sum_{n=1}^{N}\left(\underline{C/N}_2[n]-\overline{\underline{C/N}_2}\right)^2}}, -N < m < 0 \end{cases} \quad (4)$$

Here $\overline{\underline{C/N}_1}$ is the mean value of $\underline{C/N}_1$ and $\overline{\underline{C/N}_2}$ is the mean value of $\underline{C/N}_2$. We assume that the speckle patterns generated by different polarizations are highly uncorrelated and the photodetector signals from these two diversity channels are statistically independent, if the value of the cross correlation is small. We will substantiate this assumption later in section 3.1 with experimental results.

To obtain the *C/N* of the photodetector signal, the carrier and the noise power are calculated with the power spectral density (PSD) by using MATLAB function "*periodogram*". If the measuring time for calculating a PSD is very short (e.g., several or a few tens of µs), the carrier frequency can be assumed to be stationary, regardless of whether the specimen is stationary or not. Carrier power can be estimated by summing the maximum bin entry and its largest neighbor in order to avoid problems through spectral leakage [25] (see for example in figure 3). The noise power can be estimated with the sum of the amplitudes of all bins of the PSD in the demodulation bandwidth not used to estimate the signal power.

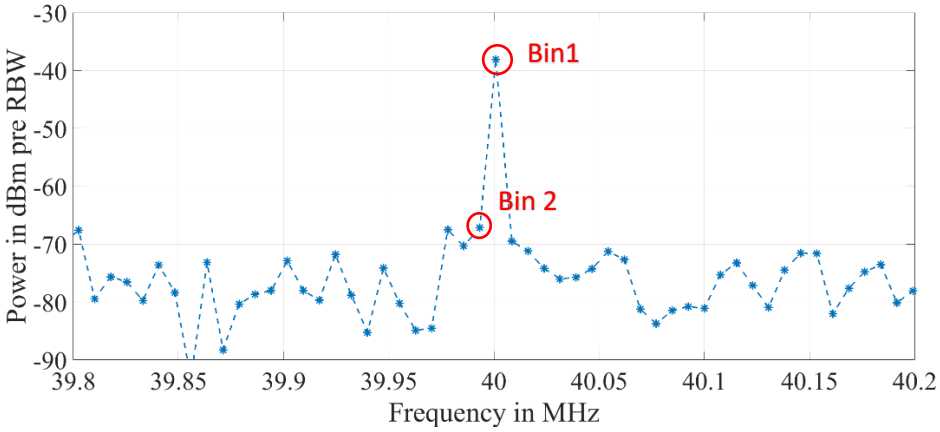

Figure 3: Power spectral density (PSD) of the photodetector signal. Resolution bandwidth (RBW) is 7.63 kHz.

For example, the carrier power in figure 3 can be calculated using the sum of Bin 1 and Bin 2, while the noise power can be calculated using sum of the remaining bins in this figure. Then the *C/N* of this photodetector signal at a demodulation bandwidth of 400 kHz is $C/N = 373.54$.

Compared to our previous setup [7] (figure 1), both the incident and the receiving beam paths of the diversity combined optical structure are changed (figure 4). A quarter-wave plate after the mirror alters the polarization of incident beams from linear to circular. Thus, both the incident beams and the scattered light contain s- and p-polarization components. The scattered light from each measuring point passes through a polarization beam splitter, then each polarization component (s- and p-polarization) is

detected by a single photodiode.

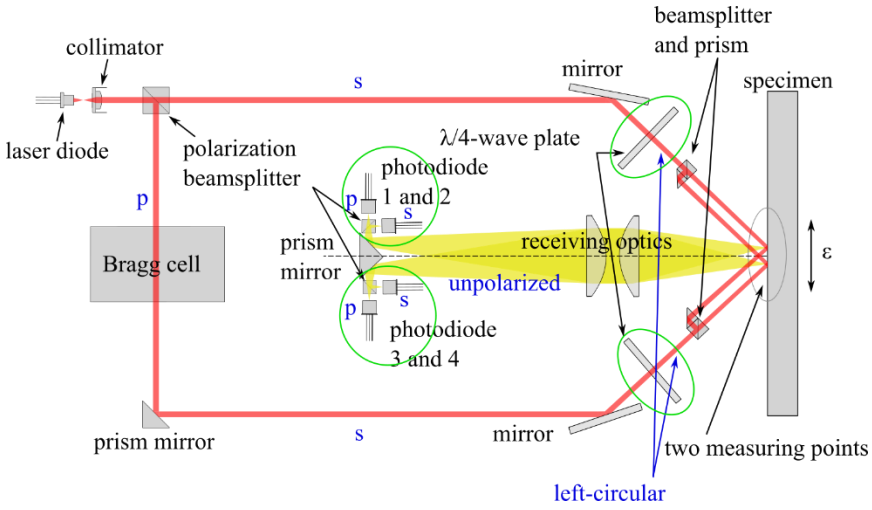

Figure 4: Schematic drawing of the new optical setup with polarization diversity. The changes compared to the previous optical setup are marked with green circles. The polarization states of the beams are shown (in blue).

The Doppler signals from both photodetectors (for each measuring point) are digitized at a sampling rate of 250 MHz. The *C/N* provides the weighting for the combination of the two signals. The carrier and the noise power can be calculated with the PSD. The segment length is the number of the samples used for one demodulation segment. A PSD is estimated for each segment. The segment is a compromise between sufficient spectral resolution of the PSD and the temporal resolution of the weighting. The larger the number of samples in a segment, the better the spectral resolution of the PSD. In contrast, weighting the two signals in a segment long enough for altering speckles can result in an average of different speckles. As a result, signal dropouts sometimes cannot be avoided. In general, a long segment length can be chosen, if the in-plane velocity of the specimen is small. A short segment length should be selected for high in-plane velocities. The combined signal V_{comb} is obtained using linear diversity combing [26] with the following equation (see for example in [21-23]) from velocity signals V_i from single photodetector

$$V_{comb} = \sum_{i=1}^{2} w_i V_i \,, \tag{5}$$

with the weighting factors

$$w_i = \frac{C/N_i^{\alpha}}{\sum_{j=1}^{2} C/N_j^{\alpha}} \,. \tag{6}$$

Here the exponent α is a factor for stronger weighting of signals with a good *C/N*. The diversity combing method is then a standard maximum radio combining (MRC) [27] when $\alpha = 1$. We tested the exponent α with different value (from 1 to 5). Generally, all results ($\alpha = 1, 2, \ldots, 5$) were almost similar. The least signal dropouts occurred for $\alpha = 3$. Therefore, the exponent α was set to 3 in the following experiment. The digitized and combined Doppler signal is mixed digitally in the baseband and IQ-demodulated [28] in a PC and, finally, the robust strain signal is calculated.

2.3 Theoretic model for estimating the probability of signal dropout

The probability density function of the intensity of laser speckles is given by the following formula (see for example the textbook of Goodman [8])

$$p(I) = \frac{1}{I_0} \cdot e^{-I/I_0} , \tag{7}$$

whereby I_0 is the mean intensity. The probability that the intensity exceeds a certain threshold can be calculated by [8]

$$P(I \geq I_t) = \int_{I_t}^{\infty} p(I)\,\mathrm{d}I = \int_{I_t}^{\infty} \frac{1}{I_0} \cdot e^{-I/I_0}\,\mathrm{d}I = e^{-I_t/I_0} , \tag{8}$$

with the certain threshold of I_t. The probability of signal dropout P_{single} of a single detector signal is then computed from

$$P_{single} = P(I < I_t) = 1 - P(I \geq I_t) = 1 - e^{-I_t/I_0} . \tag{9}$$

Here the intensity threshold I_t corresponds to the *C/N* of photodetector signal in the demodulation bandwidth equal to 1. The probability of signal dropouts P_{comb} in both independent photodetector signals is given by

$$P_{comb} = P(I_1 < I_t \cap I_2 < I_t) = P_{single}^2 = 1 - 2e^{-I_t/I_0} + e^{-2I_t/I_0} , \tag{10}$$

whereby I_1 and I_2 are the intensity of both speckle patterns. Here we assume that such individual detector signals are uncorrelated and have the same mean intensity.

Now let us establish the relationship between the probability of signal dropouts and the demodulation bandwidth. Assuming that the noise is white and, thus, the noise power in the demodulation bandwidth grows proportionally with the bandwidth. The required signal power for a *C/N* exceeding 1 also increases proportionally with the bandwidth. Thus, the intensity threshold I_t increases proportionally with the bandwidth. The probability of signal dropouts P_{single} can be given as a function of the demodulation bandwidth *B*

$$P_{single}(B) = 1 - e^{-I_{t,1\mathrm{Hz}}B/I_0} , \tag{11}$$

with $I_{t,1\mathrm{Hz}}$ the intensity threshold at a demodulation bandwidth of 1 Hz. As well, the probability of a signal dropout P_{comb} with diversity (equation 10) can be expressed as

$$P_{comb}(B) = 1 - 2e^{-I_{t,1\mathrm{Hz}}B/I_0} + e^{-2I_{t,1\mathrm{Hz}}B/I_0} . \tag{12}$$

For measuring strain, two separate measuring points with a defined distance are required. The signal dropout for strain measurement means signal dropouts occur at any of the both measuring points. Therefore, the probability of signal dropout P_{st} by strain measurement without diversity is given by

$$\begin{aligned} P_{st}(B) &= P_{single}(B) \cup P_{single}(B) = 2P_{single}(B) - P_{single}^2(B) \\ &= 1 - e^{-2I_{t,1\mathrm{Hz}}B/I_0} . \end{aligned} \tag{13}$$

Here we assume that the average received light power of both measuring points are identical and that the speckles from both measuring points are statistically independent. In the same way, the probability of signal dropouts $P_{st,comb}$ for measuring strain with diversity is computed from

$$P_{st,comb}(B) = 2P_{comb}(B) - P_{comb}^2(B) = 1 - \left(2e^{-I_{t,1\mathrm{Hz}}B/I_0} - e^{-2I_{t,1\mathrm{Hz}}B/I_0}\right)^2 . \tag{14}$$

In addition, the reduction of probability of signal dropouts ΔP_{single} for single measuring point using diversity yields

$$\Delta P_{single}(B) = P_{single}(B) - P_{comb}(B) = e^{-I_{t,1\mathrm{Hz}}B/I_0}\left(1 - e^{-I_{t,1\mathrm{Hz}}B/I_0}\right) . \tag{15}$$

The reduction of the probability of signal dropouts ΔP_{st} for strain measurement is computed from

$$\Delta P_{st}(B) = P_{st}(B) - P_{st,comb}(B) = e^{-2I_{t,1\mathrm{Hz}}B/I_0}\left(1 - e^{-I_{t,1\mathrm{Hz}}B/I_0}\right)\left(3 - e^{-I_{t,1\mathrm{Hz}}B/I_0}\right). \quad (16)$$

These two values ΔP_{single} and ΔP_{st} show how strongly the signal dropouts can be reduced.

This theoretical model is based on the speckle statistics. Therefore, it may be suitable not only for our laser extensometer with polarization diversity, but also for diversity technologies in other laser sensors. For example, equation 11, 12 and 15 can also be implemented for common LDV, which has only one measuring point, while equation 13, 14 and 16 can be easily extended to higher numbers of multiple measurement points. The most important precondition is that the speckle intensity is stochastically independent for different speckle patterns.

2.4 Experimental setup

The complete optical structure with polarization diversity was integrated into a compact housing (approx. 300×270 mm). Figure 5 shows the internal optical structure of our laser extensometer. The arrangement of the light beams is sketched, with the incident beams shown in red and the detected light in yellow.

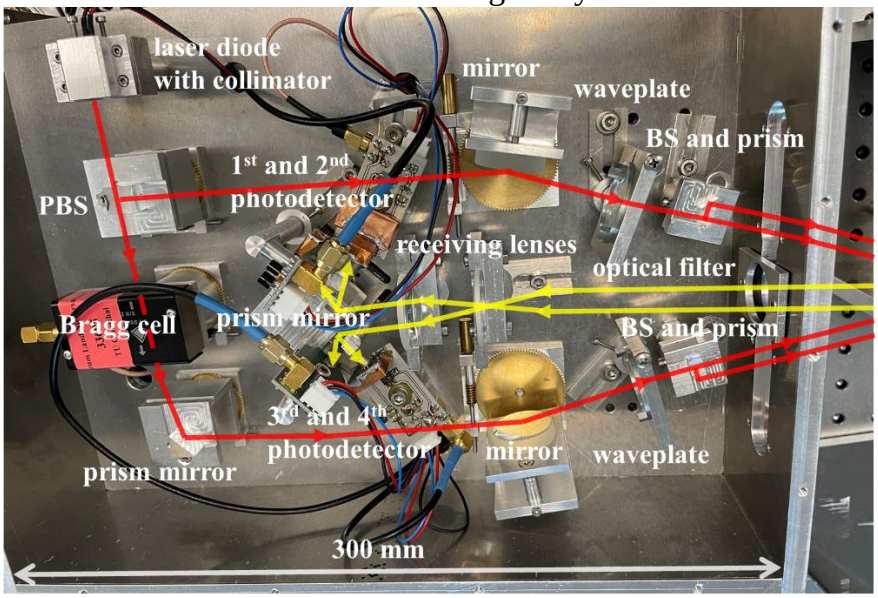

Figure 5: the internal optical structure with polarization diversity.

To explore the statistical behavior of the signal dropout, an aluminum wheel was placed in front of our laser sensor as a specimen and an in-plane motion was generated (in figure 6). The surface of the wheel was applied with retro spray. By strain measurement in a resonance test machine, the surface of specimen can also be applied with retro spray. The diameter of the wheel is 100 mm and, therefore, the rotational motion in the measurement area determined by the image area of photodiode on the wheel surface (300×300 µm) can be considered with good approximation as an in-plane motion. The distance between the two measuring points is 6 mm. A smaller wheel can negatively affect the measuring results since the assumption of a transformation of rotation to in-plane displacement is no longer accurate. The signal strength will also be reduced due to the Lambert's cosine law [29], since less light power is collected if the surface is tilted. Thus, the *C/N* is reduced in average for a larger tilt. Therefore, only a single measuring point was tested once. The second measuring point was tested after the

measurement of the first measuring point was completed.

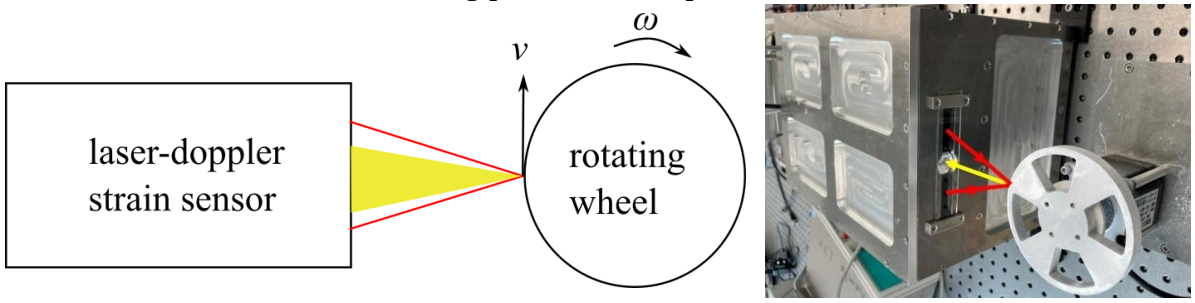

Figure 6: Schematic drawing (left) and photo (right) of the experimental setup. The direction of light beams of single measuring point is sketched, with the incident beams shown in red and the collected scattered light in yellow.

3. Results and discussion

3.1 Results of correlation experiment

Signal diversity required signals with uncorrelated noise and uncorrelated signal strengths. Therefore, we explored the correlation between these quantities first between different measurement points for the same polarization and then we investigated the correlation between signals obtained from different polarization states.

In a first experiment, the autocorrelation of $N = 1000$ measurement positions were measured to prove uncorrelated speckle fields at different measurement positions. Uncorrelated speckle fields at different measurement positions are necessary for the validity of formulas 13 and 14.

The wheel had a speed of 0.01 m/s at its circumference (of 31.4 cm). A speckle position was measured every 31.4 ms which corresponds to a displacement of 314 µm between the measurement positions. These $N = 1000$ different speckle positions were equally spaced on the surface of the disk. The width of the image area of the photodiode on the measuring surface was 300 µm. The distance between two speckle positions were a little bit larger than the image are because we wanted to ensure no overlap in adjacent speckle positions over the surface of the wheel. The measuring time for each speckle position was 0.03 ms. The in-plane displacement of the specimen during this time is about 0.3 µm (1/1000 of the speckle size). The speckles can be approximated as stationary at such a small speckle displacement which is a fraction of the speckle size. The autocorrelation $\underline{R}_{\underline{C/N}_1,\underline{C/N}_1}$ was calculated using $\underline{C/N}_1$ instead of $\underline{C/N}_2$ in equation 4 (corresponding to the cross-correlation of $\underline{C/N}_1$ and itself). Figure 7 shows this result.

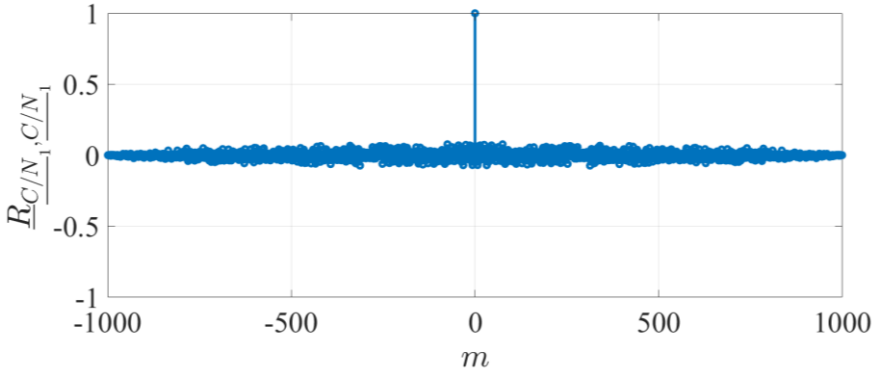

Figure 7: Autocorrelation $\underline{R}_{\underline{C/N_1},\underline{C/N_1}}$ (equation 4) of the *C/N* values of a single polarization state at $N = 1000$ different positions on the surface of the specimen with counter variable m. The demodulation bandwidth is $B = 250$ kHz.

The result of the autocorrelation demonstrates that the laser speckles of a single polarization state at different positions are spatially uncorrelated as expected. The autocorrelation is only $\underline{R}_{\underline{C/N_1},\underline{C/N_1}} = 1$ for $m = 0$ and close to zero for all other entries. Therefore, it can be assumed that the speckles at both measuring points are uncorrelated and equations 13 and 14 can be implemented for our extensometer.

In the second correlation experiment, we derived the cross-correlation between two speckle fields also at these $N = 1000$ measurement points but each for two orthogonal polarization states. The independence of the speckles from two perpendicular polarization states is the most important requirement for the new optical structure of our extensometer with polarization diversity. Therefore, we needed to prove that this is a valid assumption. The experimental setup was similar to the autocorrelation experiment, except that the cross-correlation $\underline{R}_{\underline{C/N_1},\underline{C/N_2}}$ was derived by equation 4. The results are shown in figure 8. The low value of the cross-correlation shows that highly uncorrelated speckle patterns can be produced by light with different polarizations. Thus, the polarization diversity can be implemented to reduce the speckle noise and the effects of signal dropouts.

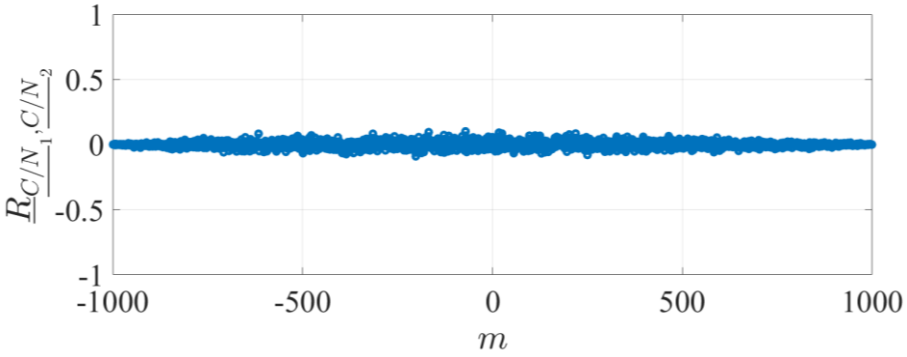

Figure 8: Cross-correlation $\underline{R}_{\underline{C/N_1},\underline{C/N_2}}$ (equation 4) of the *C/N* values of both diversity channels, which detect different polarization states, at $N = 1000$ different positions on the surface of the specimen with counter variable m. The demodulation bandwidth is $B = 250$ kHz.

3.2 Statistical results of reducing signal dropouts

In this part, we prove that our mathematic model for estimating the probability of signal dropouts depending on the demodulation bandwidth is in good agreement with the experimental results. In the experiment, the demodulation bandwidth was determined by the digital FIR-filter before demodulating. In total, 150 different demodulation bandwidths (from 70 kHz to 10 MHz) were tested. For our experimental setup, the measured probability of signal dropouts is almost zero at a bandwidth < 70 kHz and is almost one at bandwidth > 10 MHz. Like the correlation experiment, the wheel rotated also with a linear velocity of 0.01 m/s. A speckle position was measured every 31.4 ms. In total, 1000 equally spaced different speckle positions on the surface of the specimen were chosen.

Signal Diversity with two Polarization States for a Single In-Plane-LDV Channel

The theoretical probability of signal dropouts P_{single} for a single detector signal can be calculated using formula 11 and the theoretical probability P_{comb} for the diversity combined signal can be calculated using formula 12. The term $I_{t,1\mathrm{Hz}}/I_0$ in both equations (11 and 12) is influenced by many different parameters, such as the power of incident light, the scattering efficiency, the image area of photodiode on the measuring surface, the solid angle of the receiving lenses, and much more. Therefore, it is quite difficult to calculate this term by theoretical considerations. On the other hand, it can be straight forward estimated from measuring results by rearranging equation 11. The term $I_{t,1\mathrm{Hz}}/I_0$ can be estimated with these 4×150 measuring results by evaluating the equation

$$I_{t,1\mathrm{Hz}}/I_0 = -\frac{1}{600}\sum_{\mathrm{j}=1}^{4}\sum_{i=1}^{150}\frac{1}{B[i]}\cdot \ln\left(1 - P_{single,exp}[i,j]\right), \qquad (17)$$

where $P_{single,exp}[i,j]$ is the probability of signal dropouts for the j-th detector signal (4 detectors in total, for 2 measuring points and 2 polarization states) at the demodulation bandwidth $B[i]$. 150 different bandwidths in total were evaluated. Then, this estimated value of $I_{t,1\mathrm{Hz}}/I_0$ can be inserted in equation 11 to calculate the theoretical probability of signal dropouts P_{single} for single detector signal, and in equation 12 to calculate the probability P_{comb} for the diversity combined signal, at the demodulation bandwidth B from 70 kHz to 10 MHz. P_{single} and P_{comb} were plotted in figure 9.

At the demodulation bandwidth $B[i]$, the relative frequency of signal dropouts $P_{single,exp}[i,j]$ for j-th detector signal derived by the $N = 1000$ independent speckle positions at the same polarization state was computed from

$$P_{single,exp}[i,j] = \frac{\text{Number of signal dropouts}}{1000}.$$

Similarly, the relative frequency of dropouts $P_{comb,exp}[i,l]$ for diversity combined signal was given by

$$P_{comb,exp}[i,l] = \frac{\text{Number of signal dropouts}}{1000}.$$

Here $l = 1$ or 2 corresponds to two measuring points of our extensometer. The relative frequencies at experiments $P_{single,exp}$ from all four single detector signals were identical. The relative frequencies $P_{comb,exp}$ from both measuring points were also identical. Therefore, two dashed curves of the relative frequency of dropouts were plotted in figure 8. One curve is the relative frequency of dropouts

$$P_{single,exp} = \frac{1}{4}\sum_{j=1}^{4} P_{single,exp}[j]$$

for single detector signal. The other curve is the relative frequency

$$P_{comb,exp} = \frac{1}{2}\sum_{l=1}^{2} P_{comb,exp}[l]$$

for the diversity combined signal. Figure 8 shows the dependence of the theoretical probability and the experimental relative frequency of dropouts on the demodulation bandwidths.

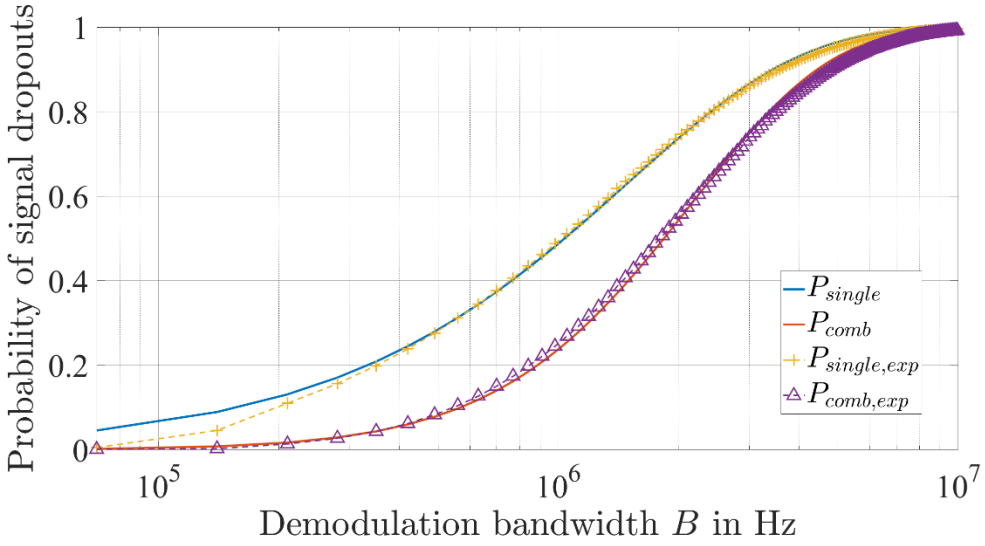

Figure 9: The relative frequency at experiments and the probability derived from the statistic model for the signal dropouts in relation to the demodulation bandwidth B at a single measurement point to demonstrate the effect of polarization signal diversity for a single laser-Doppler, in-plane channel. The theoretical estimated probability (P_{single} in equation 11 and P_{comb} in equation 12) are plotted in solid lines and the relative frequency at experiments ($P_{single,exp}$ and $P_{comb,exp}$) are shown by dashed lines with different shapes. Every shape describes an experimental value.

From this figure, the experimental results are generally in good agreement with the theoretical values. Comparing the results with and without diversity, our polarization diversity structure can substantially reduce signal dropouts.

Signal Diversity with two Polarization States for a Two-Point Laser Extensometer

The theoretical probability (P_{st} and $P_{st,comb}$) and the experimental relative frequency of signal dropouts ($P_{st,exp}$ and $P_{st,comb,exp}$) are evaluated to investigate the effects of polarization diversity for strain measurements obtained from two measurement positions. The theoretical probability P_{st} (without diversity) was calculated using formula 13 and $P_{st,comb}$ (with polarization diversity) was calculated using formula 14 at the demodulation bandwidth of 70 kHz to 10 MHz. The term $I_{t,1\mathrm{Hz}}/I_0$ in both equations (13 and 14) was also determined by equation 17. Since the both measuring points were not tested simultaneously, the relative frequency of signal dropouts $P_{st,exp}$ for strain measurement without diversity was calculated using the relative frequencies from both measuring points ($P_{single,exp,1st}$ for the first measuring point and $P_{single,exp,2nd}$ for the second) by

$$\begin{aligned} P_{st,exp} &= P_{single,exp,1st} \cup P_{single,exp,2nd} \\ &= P_{single,exp,1st} + P_{single,exp,2nd} - P_{single,exp,1st} \cdot P_{single,exp,2nd} \end{aligned} \tag{18}$$

with

$$P_{single,exp,1st} = \frac{1}{2}\sum_{j=1}^{2} P_{single,exp}[j]\,,$$

and

$$P_{single,exp,2nd} = \frac{1}{2}\sum_{j=3}^{4} P_{single,exp}[j]\,.$$

$P_{single,exp}[j]$ is the relative frequency of signal dropouts of j-th detector. Photodetector 1 and 2 are for the first measuring point and photodetector 3 and 4 for the second.

For the case with diversity, the relative frequency of dropouts $P_{st,comb,exp}$ at each demodulation bandwidth is calculated using

$$P_{st,comb,exp} = P_{comb,exp,1} \cup P_{comb,exp,2} = P_{comb,exp,1} + P_{comb,exp,2} - P_{comb,exp,1} \cdot P_{comb,exp,2} \,. \quad (19)$$

$P_{comb,exp,1}$ is the measured relative frequency of dropouts with diversity for the first measuring point and $P_{comb,exp,2}$ is that for the second measuring point. Here we assume that the speckles at both measuring points are stochastically independent, since the result of the autocorrelation experiment in 3.1 demonstrates the speckles at both measuring points are uncorrelated. The probability (P_{st} and $P_{st,comb}$) and relative frequency of signal dropouts ($P_{st,exp}$ and $P_{st,comb,exp}$) in relation to the demodulation bandwidth B is shown in figure 10.

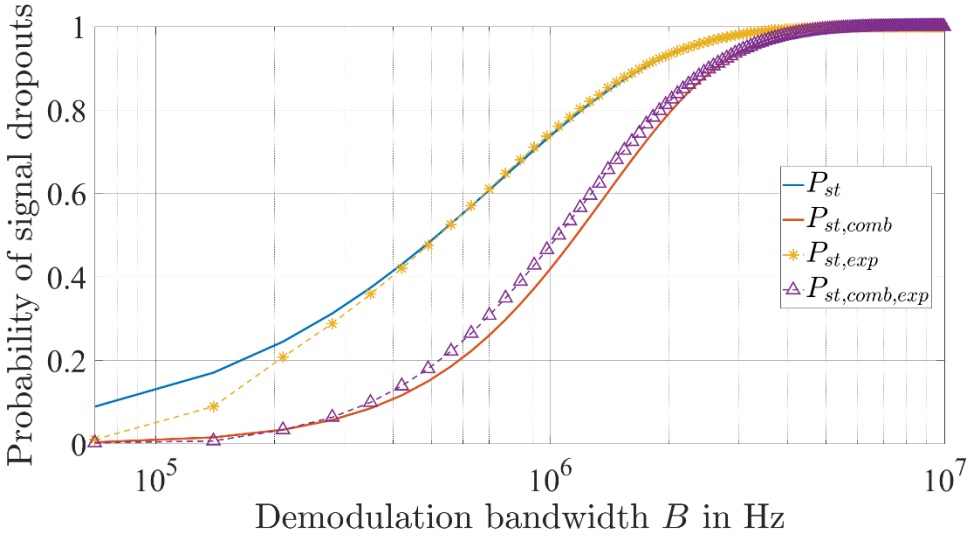

Figure 10: The relative frequency at experiments and the probability of signal dropouts derived from the statistic model in relation to the demodulation bandwidth B for strain measurement to demonstrate the effect of polarization signal diversity for the laser extensometer. The theoretical estimated probabilities (P_{st} from formula 10 and $P_{st,comb}$ from formula 11) are plotted in solid lines and the relative frequency from experimental results ($P_{st,exp}$ and $P_{st,comb,exp}$) are shown by dashed lines with different shapes. Every shape describes an experimental value.

The relative frequency at experiments in figure 10 generally matches the theoretically estimated probability dependent on the demodulation bandwidth quite well. Our findings prove that polarization diversity technology can dramatically reduce the occurrence of signal dropouts for our laser extensometer. Moreover, it can be observed that the experimental relative frequency of signal dropouts $P_{st,comb,exp}$ for the diversity combined signal is slightly above the theoretical probability $P_{st,comb}$. We think that the main reason for this may be the temporal resolution of the weighting. In this experiment, the measurement data (the photodetector signal) in every 0.03 ms was used to calculate a single power spectral density (PSD) and the *C/N*. The algorithm of combining single detector signals (equation 5) averaged all the speckles in such a duration of 0.03 ms (corresponding to a displacement of the surface of the specimen of 0.3 µm). Some signal dropouts can therefore not be avoided. In fact, this phenomenon also exists in figure 9 (the case of a single measuring point), but is inconspicuous.

The reduction in signal dropouts (ΔP_{single} in equation 15 for a single measuring point and ΔP_{st} in equation 16 for strain measurement with two measuring points) can be

identified even more clearly in figure 11.

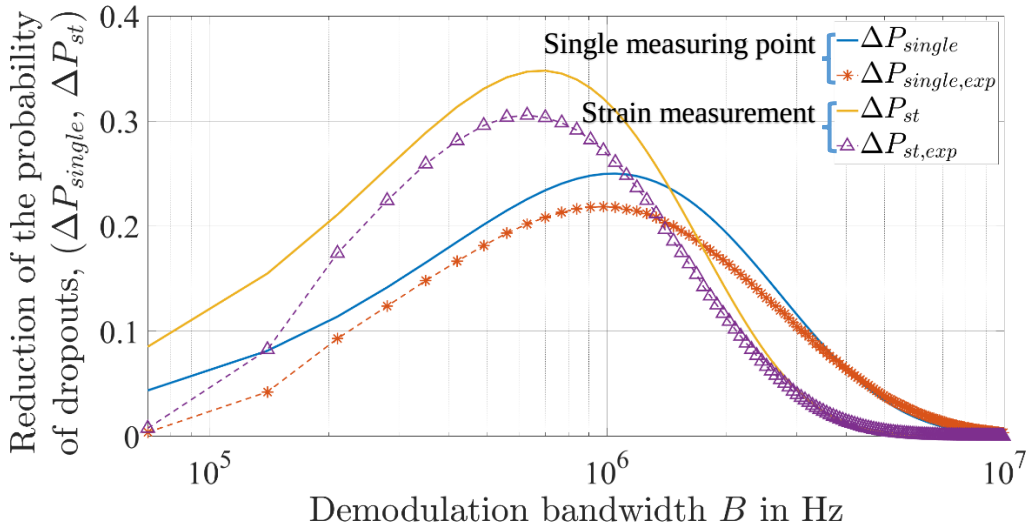

Figure 11: Reduction of the probability of dropouts ΔP_{single} (for a single measuring point) and ΔP_{st} (strain measurement) in relation to the demodulation bandwidth B. The theoretical estimated value (ΔP_{single} in equation 15 and ΔP_{st} in equation 16) are plotted in solid lines and the experimental value ($\Delta P_{single,exp}$ and $\Delta P_{st,exp}$) are shown by dashed lines with different shapes. Every shape describes an experimental value.

From this figure, the tendency of the experimental results ($\Delta P_{single,exp}$ and $\Delta P_{st,exp}$) highly matches the theoretical model (ΔP_{single} and ΔP_{st}). The slight differences between experiments and simulation is probably due to the limited temporal resolution of the weighting. At a lower demodulation bandwidth, the diversity technology reduces the probability of signal dropouts in strain measurement (in the case of multiple measurement points) more efficiently than in the case of a single measurement point. However, at a larger bandwidth, signal combining is more efficient for a single measuring point.

Diversity technology can only improve signal quality if at least one channel has sufficient signal strength. Thus, at very large bandwidths noise may be too strong to enable an improvement through signal combining as figure 11 demonstrates. In addition, there is no improvement for reducing the dropouts at small bandwidths because the single signal had already a good quality. This conclusion seems to be correct also according to the theoretical model (equation 15 and 16). When the term $I_{t,1\mathrm{Hz}}B/I_0$ in equation 15 and 16 converges to zero or to infinity, ΔP_{single} and ΔP_{st} converge to zero. It can be concluded, that there is an optimal range for the bandwidth for every sensor and channel number for combination to reduce the probability of signal dropout. Diversity technology can substantially improve signal quality, if $I_{t,1\mathrm{Hz}}B/I_0$ converges to zero. In this case, there are almost no signal dropouts in the detector signal. Diversity technology reduces also the speckle noise and improves the noise-limited resolution of the out-of-plane LDV [21-23] for measurements on a single position. This is also true for in-plane LDV. Our results can be transferred to all other cases for Laser-Doppler sensors where one or more than one measurement point is required.

3.3 Reduction of signal dropouts and speckle noise in time domain

In the next step, we want to present noise reduction by signal diversity in the time domain. In the following experiment, the wheel rotation resulted in a constant velocity of 0.1 m/s at its circumference. At a large in-plane velocity, signal dropouts occur more frequently in the time domain because the speckle position changes rapidly. If the velocity was also 0.01 m/s, as in the statistical experiment above, a dropout might not occur during a long measuring time. The demodulation bandwidth was set at $B = 250$ kHz. The segment length sl for estimating PSD was $sl = 2^{11}$. The figure 12 shows the photodetector signals and the demodulated velocity-/displacement-signals in the time domain. Due to the huge amount of data, only a 4 ms long excerpt from the data set was plotted.

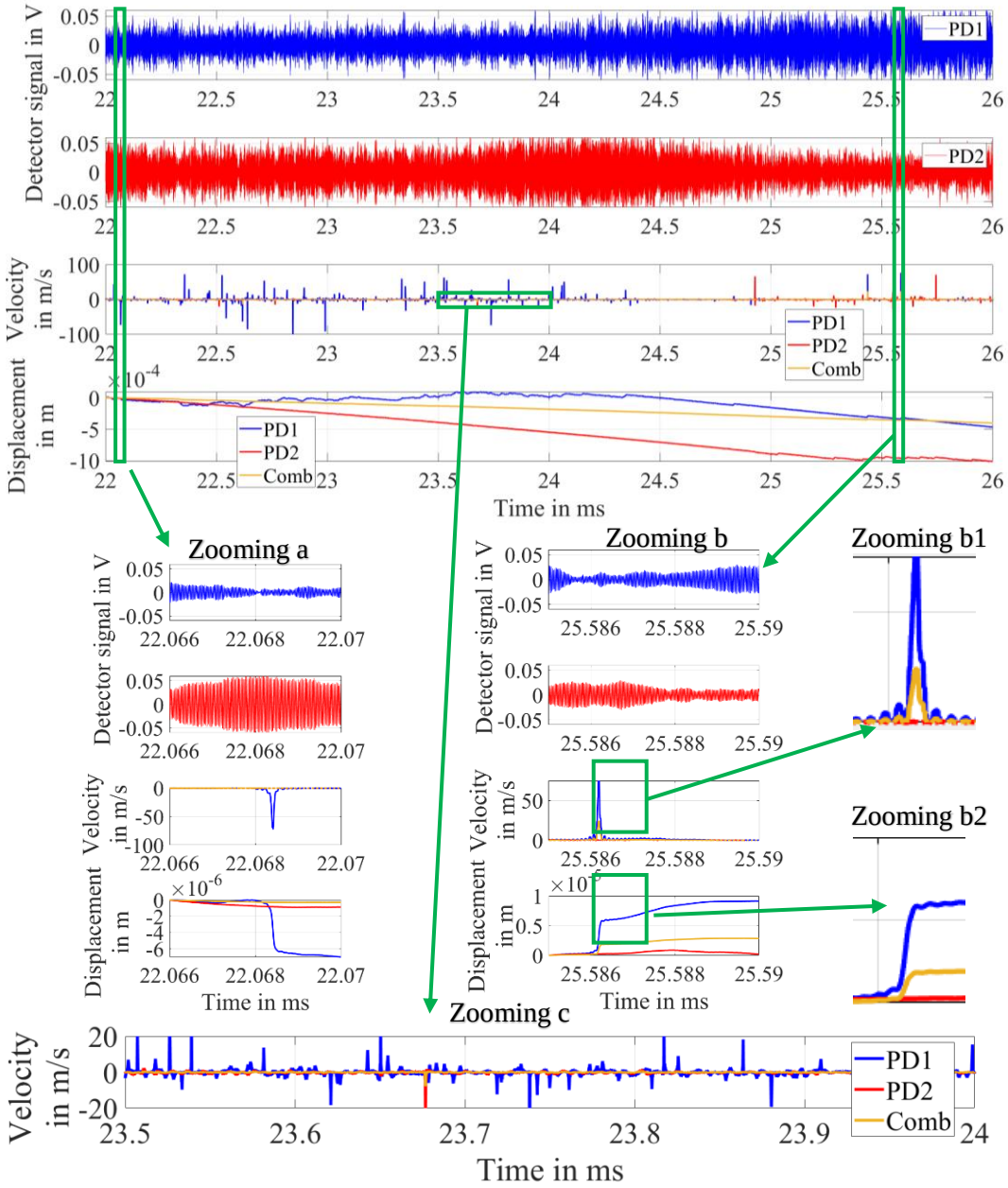

Figure 12: The photodetector signals (PD1 and PD2), the demodulated velocity signals and the displacement signals at a demodulation bandwidth of 250 kHz. The demodulation results from each individual photodetector signal (PD1 and PD2) and diversity combined signal (Comb) are provided.

Two locations of signal dropout were shown with zooming (a, b, b1 and b2). The velocity signal was also zoomed (c). The displacement values of all figures were set to zero at the beginning.

In general, multiple signal dropouts (corresponding to noise bursts in velocity signal and phase distortions in displacement signal) were detected from each photodetector during this 4 ms. However, there were no significant noise bursts and phase distortions in the diversity combined signal (Comb). Thus, the signal dropouts by individual detector signal can be avoided and do not affect the measurement result.

At zooming a, a signal dropout was observed by a single detector signal (PD1) during 22.068 ms and 22.07 ms. The Doppler signal from another detector (PD2) was very strong at the same moment. There was no significant dropout in the diversity combined signal (Comb). As mentioned earlier, signal dropouts sometimes cannot be avoided due to the limited temporal resolution of the weighting. A signal dropout was observed in a single detector signal (PD1). Although there was no dropout by the other detector signal (PD2), the dropout remained by the combined signal. In this experiment, a segment length of $sl = 2^{11}$ was chosen for estimating the PSD. As a result, the PSD was estimated using samples between 25.582 ms and 25.59 ms. The signal strength of two channels varied during this 0.08 ms. There was no significant difference in the average signal strength between both channels and, consequently, the two weighting factors in equation 2 were almost the same. Using equation 4, the combined velocity signal in this segment was about half of the sum of the velocity signals from both photodetectors. Thus, this signal dropout retained by the combined signal but its reduction is a positive effect of signal combining.

3.4 Results of strain measurement

Finally, the results of strain measurement are presented. A thin aluminum plate was used as the specimen in this experiment. The surface of the plate was applied with retro spray. The experimental setup is shown in figure 13. One side of the specimen was fixed. An initial force was applied to the other side of the specimen to generate an initial strain. During the measurement, the specimen was freely damped. Therefore, a strain signal in the form of a freely damped sine wave could be expected.

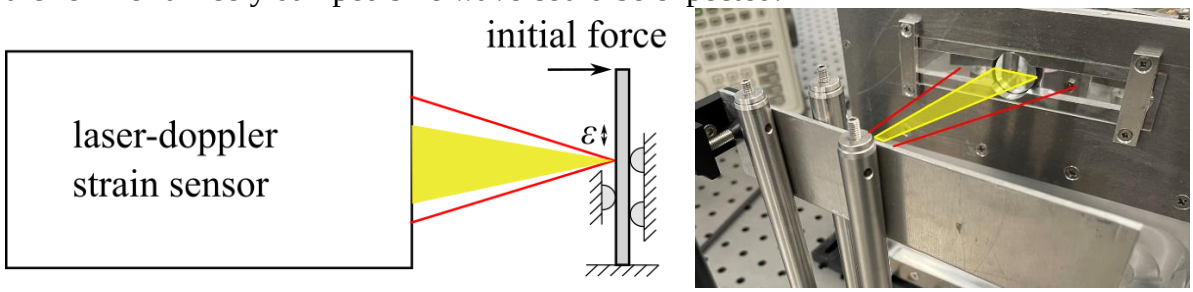

Figure 13: Schematic drawing (left) of the experimental setup for measuring strain and photo (right) of the specimen (right). The direction of light beams is sketched, with the incident beams shown in red and the scatted light in yellow.

Figure 14 shows the demodulated strain signal in the time domain (left) and its spectrum (right). Because of the huge data rate, only 1 s data is plotted. Only the strain signal with diversity is plotted in the time domain, since the measuring results without and with diversity are almost identical. In this case, the *C/N* of all four detector signals during the measurement were above 10^3 and no signal dropout occurred.

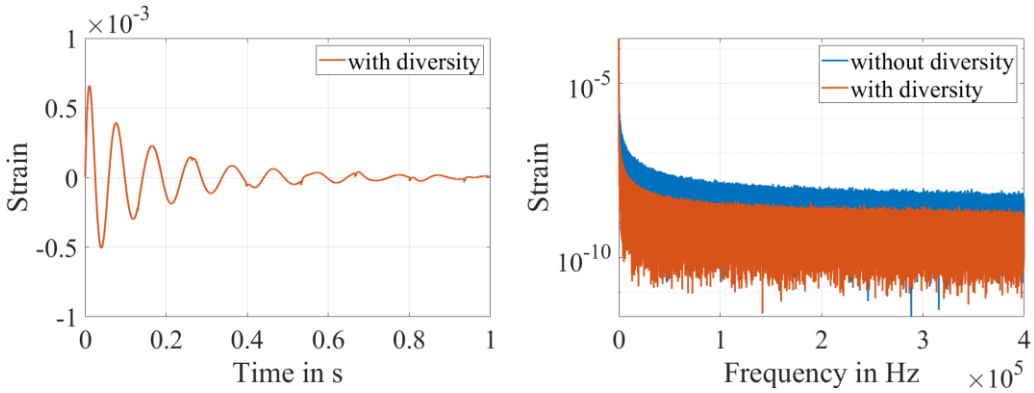

Figure 14: Demodulated strain signal (left) and its spectrum (right). Demodulation bandwidth is 250 kHz. The resolution bandwidth (RBW) of the spectrum is 1 Hz.

Here, the results without diversity were demodulated from photodetector 1 at the first measuring point and photodetector 3 at the second. The results with diversity were demodulated using diversity combined signals. The spectrum shows that the speckle noise of the diversity combined signal can be significantly reduced, even though the *C/N* of the single detector signals was already good before the signal combination.

4. Conclusions and outlook

In summary, we successfully improved our laser-Doppler extensometer employing polarization diversity. The implemented methods reduce signal dropouts and noise substantially. A theoretical model based on speckle statistics is constructed to estimate the probability of signal dropouts. The model is not only suited for our laser Doppler extensometer with polarization diversity, but also for other laser-Doppler sensors employing different signal-diversity solutions. The relationship between the probability of signal dropouts and the demodulation bandwidth was studied. The experimental results are in high agreement with the theoretical probability of signal dropouts. Polarization diversity can, therefore, substantially reduce the occurrence of dropouts at a certain optimal range of the demodulation bandwidth. Diversity technology can only improve signal quality if at least one channel has sufficient signal strength. At very large bandwidths noise may be too strong to enable an improvement by using diversity. At small bandwidths (almost no signal dropout), diversity technology can still improve signal quality. The speckle noise in the demodulated signal can be significantly reduced with our signal-diversity technique, even though no signal dropout occurs.

So far, we have established the mathematical model for the probability of signal dropouts considering only the photodetector signal. All the signals, where the *C/N* above 1 (fm threshold), were considered equally. In the future, we may extend our model to estimate the theoretical reduction of speckle noise in the demodulated signal.

Future work is directed towards further improvements of the optics design in order to gain more sensitivity by collecting light even more efficient as our sensor already does.

Funding: This project is funded by the BMWK program "Zentrales Innovationsprogramm Mittelstand-ZIM". ZIM grant number: ZF4314303 SN9. We acknowledge support by Open Access Publishing Fund of Clausthal University of Technology.

Conflicts of Interest: The authors declare no conflict of interest. The funders had no role in the design of the study; in the collection, analyses, or interpretation of data; in the writing of the manuscript, or in the decision to publish the results.

Reference

1. H.-E. Albrecht, I.M. Borys, D.-I.N. Damaschke, I.C. Tropea, Basic Measurement Principles, in: Laser Doppler and Phase Doppler Measurement Techniques, Springer Science and Business Media LLC: Cham, Switzerland, 2003, pp. 9–26. DOI: 10.1007/978-3-662-05165-8_2.
2. B.E. Truax, F.C. Demarest, G.E. Sommargren, Laser Doppler velocimeter for velocity and length measurements of moving surfaces, Applied Optics 23 (1) (1984) 6–73. DOI: 10.1364/AO.23.000067.
3. Y. Zhong, G. Zhang, C. Leng, T. Zhang, A differential laser Doppler system for one-dimensional in-plane motion measurement of MEMS, Measurement 2007, 40, 623–627. DOI: 10.1016/j.measurement.2006.07.006
4. S. Mekid, K. Vacharanukul Differential Laser Doppler based Non-Contact Sensor for Dimensional Inspection with Error Propagation Evaluation, Sensors 2006; 6(6):546-556. DOI: 10.3390/s6060546
5. D. Kohlmann, H. Wulfmeier, M. Schewe, C. Rembe, H. Fritze, Chemische Ausdehnung von Sensor- und Elektrolytmaterialien bei hohen Temperaturen, in: 15. Dresdener Sensor-Symposium 2021. DOI: 10.5162/15dss2021/7.2
6. C. Rembe, S. Boedecker, A. Dräbenstedt, F. Pudewills, G. Siegmund, Heterodyne laser-Doppler vibrometer with a slow-shear-mode Bragg cell for vibration measurements up to 1.2 GHz, In: Proc. SPIE 7098, Eighth International Conference on Vibration Measurements by Laser Techniques: Advances and Applications, 70980A (17 June 2008). DOI: 10.1117/12.802930
7. F. Wang, S. Krause, J. Hug, C. Rembe, A Contactless Laser Doppler Strain Sensor for Fatigue Testing with Resonance-Testing Machine, Sensors 2021, 21(1), 319, DOI: 10.3390/s21010319.
8. J. W. Goodman, Speckle phenomena in optics: theory and applications, second Edition, SPIE PRESS: Bellingham, Washington, USA, 2020.
9. J. R. Carson, Notes on the Theory of Modulation, in: Proceedings of the Institute of Radio Engineers, vol. 10, no. 1, pp. 57-64, Feb. 1922. DOI:10.1109/JRPROC.1922.219793
10. G. D. Arndt, F. J. Loch, A Study of FM Threshold Extension Techniques, NASA Technical Report, Manned Spacecraft Center, Houston, Texas, 1972.
11. J.-R. Ohm, H. D. Lüke, Analoge Modulationsverfahren, in: Signalübertragung - Grundlagen der digitalen und analogen Nachrichtenübertragungssysteme, 11th edition, Springer Berlin Heidelberg, 2010; pp. 353-377. DOI: 10.1007/978-3-642-10200-4
12. B. Li, J.-W. Liang, C.-Y. Yin, Study on the measurement of in-plane displacement of solid surfaces by laser Doppler velocimetry, in: Optics & Laser Technology, Volume 27, Issue 2, 1995, pp. 89-93, DOI: 10.1016/0030-3992(95)93620-7.
13. G. Massimiliano, M. R. Gian, The influence of operating conditions on the accuracy of in-plane laser Doppler velocimetry measurements, Measurement, Volume 26, Issue 3, 1999, Pages 207-220, DOI: 10.1016/S0263-2241(99)00041-X.
14. S. J. Rothberg, M.S. Allen, P. Castellini, D. Di Maio, J.J.J. Dirckx, D.J. Ewins, B.J. Halkon, P. Muyshondt, N. Paone, T. Ryan, H. Steger, E.P. Tomasini, S. Vanlanduit, J.F. Vignola, An international review of laser Doppler vibrometry: Making light work of vibration measurement, Optics and Lasers in Engineering, Volume 99, 2017, Pages 11-22, DOI: 10.1016/j.optlaseng.2016.10.023.
15. S. Rothberg, Numerical simulation of speckle noise in laser vibrometry, Appl. Opt. 45, 4523–4533 (2006). DOI: 10.1364/AO.45.004523
16. P. Martin, S. Rothberg, Introducing speckle noise maps for Laser Vibrometry, Optics and Lasers in Engineering, Volume 47, Issues 3–4, 2009, Pages 431-442, DOI: 10.1016/j.optlaseng.2008.06.010.
17. T. Lv, X. Han, S. Wu, Y. Li, The effect of speckles noise on the Laser Doppler Vibrometry for remote speech detection, Optics Communications, Volume 440, 2019, Pages 117-125, DOI: 10.1016/j.optcom.2019.02.014.

18. H. Beverage, H. Peterson, Diversity Receiving System of R.C.A., Communications, Inc. for Radiotelegraphy. Proc. Inst. Radio Eng. 1931, 19, 529–561. DOI: 10.1109/JRPROC.1931.222362.
19. C.M. Mclntyre, J.H. Churnside, Diversity arrays for optical communications through atmospheric turbulence, SPIE Laser Fiber Commun. 1978, 150, 2231–2258. DOI: 10.1117/12.956704.
20. K. Xu, B. Jiang, Z. Su, S. Wang, M. Guo, X. Li, Z. Du, High frequency communication network with diversity: System structure and key enabling techniques, China Communications, vol. 15, no. 9, pp. 46-59, Sept. 2018, DOI: 10.1109/CC.2018.8456451.
21. A. Dräbenstedt, Diversity Combining in Laser Doppler Vibrometry for Improved Signal Reliability, AIP Conference Proceedings 1600, 263 (2014). DOI: 10.1063/1.4879592
22. C. Rembe, A. Dräbenstedt, Speckle-Insensitive Laser-Doppler Vibrometry with Adaptive Optics and Signal Diversity, Proc. Sens. 2015, 2015, 878–883. DOI: 10.5162/sensor2015/D1.1
23. M. Schewe, C. Rembe, Signal Diversity for Laser-Doppler Vibrometers with Raw-Signal Combination, Sensors 2021, 21(3), 998, DOI: 10.3390/s21030998.
24. C. Rembe, R. Kowarsch, W. Ochs, A. Dräbenstedt, M. Giesen, M. Winter, Optical three-dimensional vibrometer microscope with picometer-resolution in x, y, and z, Optical Engineering 53(3), 034108 (26 March 2014). DOI: 10.1117/1.OE.53.3.034108
25. P. Gaydecki, Discrete Fourier properties and processing, in: Foundations of Digital Signal Processing: Theory, Algorithms and Hardware Design, the Institution of Engineering and Technology: London, United Kingdom, 2004; pp. 219-220.
26. D. G. Brennan, Linear Diversity Combining Techniques, in: Proceedings of the IRE, vol. 47, no. 6, pp. 1075-1102, June 1959, DOI: 10.1109/JRPROC.1959.287136.
27. M. Gans, The Effect of Gaussian Error in Maximal Ratio Combiners, in: IEEE Transactions on Communication Technology, vol. 19, no. 4, pp. 492-500, August 1971, DOI: 10.1109/TCOM.1971.1090666.
28. C. Rembe, G. Siegmund, H. Steger, M. Wörtge, Measuring MEMS in Motion by Laser Doppler Vibrometry, in: Optical Science and Engineering, Informa UK Limited: London, UK, 2006; pp. 245–292. DOI: 10.1201/9780429186738-11
29. E. W. Ciurczak, D. A. Burns, Handbook of Near-Infrared Analysis, second Edition. United States: Taylor & Francis, (2001).